Covalent Binding of Nanoliposomes to the Surface of Magnetotactic Bacteria for the Synthesis of Self-Propelled Therapeutic Agents

Samira Taherkhani,[†,‡] Mahmood Mohammadi,[†] Jamal Daoud,[‡] Sylvain Martel,[†,*] and Maryam Tabrizian[‡,§,*]

[†]NanoRobotics Laboratory, Department of Computer and Software Engineering, Institute of Biomedical Engineering, Polytechnique Montréal, Montréal, Québec, Canada H3C3A7, [‡]Department of Biomedical Engineering, Faculty of Medicine, McGill University, Montréal, Québec, Canada H3A2B4, and [§]Faculty of Dentistry, McGill University, Montréal, Québec, Canada H3A0C7

ABSTRACT The targeted and effective delivery of therapeutic agents remains an unmet goal in the field of controlled release systems. *Magnetococcus marinus* MC-1 magnetotactic bacteria (MTB) are investigated as potential therapeutic carriers. By combining directional magnetotaxis—microaerophilic control of these self-propelled agents, a larger amount of therapeutics can be delivered surpassing the diffusion limits of large drug molecules toward hard-to-treat hypoxic regions in solid tumors. The potential benefits of these carriers emphasize the need to develop an adequate method to attach therapeutic cargos, such as drug-loaded nanoliposomes, without substantially affecting the cell's ability to act as delivery agents. In this study, we report on a strategy for the attachment of liposomes to MTB (MTB—LP) through carbodiimide chemistry. The attachment efficacy, motility, and magnetic response of the MTB—LP were investigated. Results confirm that a substantial number of nanoliposomes (~70) are efficiently linked with MTB without compromising functionality and motility. Cytotoxicity assays using three different cell types (J774, NIH/3T3, and Colo205) reveal that liposomal attachments to MTB formulation improve the biocompatibility of MTB, whereas attachment does not interfere with liposomal uptake.

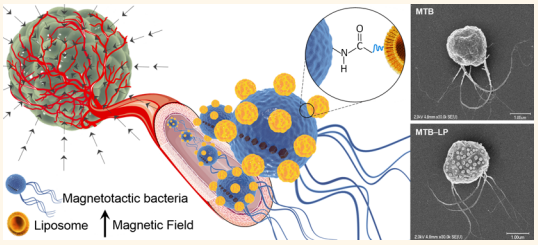

KEYWORDS: magnetotactic bacteria · nanoliposome · bioconjugation · carbodiimide chemistry · self-propelled targeted delivery · biomicrocarrier

Over the past several decades, various systems for the delivery of therapeutic agents such as polymeric micro/nanoparticles,[1] liposomes,[2] and magnetic-based nanoparticles,[3] relying on active or passive targeting mechanisms[4] of therapeutics, have been designed and evaluated in animal models as well as in clinical trials.[5] However, nonspecific distribution throughout the systemic circulation can still cause substantial toxicity and adverse side effects.[6] Among nanosized delivery systems, liposomes[2] are of particular interest, since they are biocompatible, exhibit low immunogenicity and high flexibility, protect the body from potentially toxic cargo, shield therapeutic agents from premature degradation, control release kinetics,[7] and may concurrently encapsulate a multitude of hydrophilic and/or hydrophobic drug cargos, pharmaceutical ingredients, imaging agents,[8] and genetic material by virtue of their aqueous interior and lipid exterior.[3,9] Drawbacks of the systemic application of liposomes include poor pharmacokinetic profiles, incomplete local targeting, lack of deep tissue penetration, nonspecific biodistribution, and limited retention at sites of delivery.[10] The suboptimal concentration of such therapeutic agents reaching the region to be treated cannot generally diffuse deeper in the interstitial space due to a lack of flow caused by the Tumor Interstitial Fluid Pressure (TIFP).[11] Therefore, conventional administration of such liposome-based systems often requires sustained levels of drugs to achieve therapeutic efficacy. Further from the diffusion limit of larger drug molecules, hypoxic microenvironments of tumors with approximately <0.7% O_2, resulting from oxygen consumption caused by the rapid proliferation of cancer cells,[12] are more

* Address correspondence to sylvain.martel@polymtl.ca, maryam.tabrizian@mcgill.ca.

Received for review February 25, 2014 and accepted March 31, 2014.

Published online March 31, 2014
10.1021/nn5011304

resistant and highly difficult to treat. Such lack of oxygenated regions not only impede radiotherapy treatments,[13] but chemotherapy as well, since hypoxic cells are distant from blood vessels and beyond the diffusion limit of larger drug molecules.[10,12] One strategy to minimize adverse side effects and enhance the therapeutic index in hypoxic regions is the use of targeting agents with propelling capabilities that can counteract TIFP effects, following a directionally guided transit toward the tumor with the additional capability of the agent to seek the hypoxic regions prior to the release of the therapeutics.[14] Self-propelled agents capable of some autonomy in navigating pathways, such as flagellated bacteria, could be potential candidates for targeted delivery to deep tumors. To date, bacteria including *Escherichia coli*,[15] *Salmonella*,[16] and other genera have been shown to preferentially accumulate in tissues by aerotaxis or chemotaxis suggesting the potential application of bacterial-based therapeutics. Although these bacteria can be used as therapeutic agents, they are not compatible with computer-based navigation toward tumoral regions, which would most likely enhance targeting efficacy.

In addition, to navigate and transport therapeutic agents within low Reynolds hydrodynamic conditions, such as the microvasculature (blood flow of few mm s^{-1} and diameter of approximately 4–8 μm),[17] and to reach deep inside tumors, a controllable propulsion and steering system with an appropriate size is required. Microcarriers should not exceed 2 μm in diameter.[18–20] Moreover, since the size of the openings in leaky tumor vessels are typically less than 2 μm in diameter between endothelial cells,[21] the maximum diameter of each navigable microrobotic agent must remain below 2 μm if such openings are to be exploited to enhance targeting deeper within solid tumors.

To address this issue, flagellated *Magnetococcus marinus* MC-1 magnetotactic bacteria (MTB)[22] with computer-based navigation compatibility along with appropriate steering and propulsion kinetics have been identified as such potential delivery agents with the aforementioned functionalities.[19] The combination of a flagella attached to a round cell body with a diameter around 1 to 2 μm is ideal for transiting effectively in the microvasculature, the angiogenesis network, and the interstitial space of solid tumors. Two bundles of flagella enable an average initial swimming velocity of approximately 200 μm s^{-1} (100–150 body (cell) lengths/s). Self-propulsion properties also enable the bacteria to penetrate regions that are inaccessible by passive therapies.[19] A chain of iron oxide nanoparticles, known as magnetosomes,[23,24] allows magnetotaxis control to entail such bacterial cells to aggregate in a specific region within 3D volume time-varying magnetic field sequences[25] prior to rely on the microaerophilic behavior of the MTB to target hypoxic regions. One of the many critical steps toward the potential use of such a carrier for delivering therapeutics is to develop a method of loading the bacteria while maintaining its capability for deep targeting of solid tumors.

The approach presented herein relies on the fact that amine groups on the surface of Gram-negative bacteria cells,[26] such as MC-1 MTB, enable them to covalently attach to various compounds, such as carboxylated liposomes, to allow design of the powerful targeted delivery systems. This is the grounding hypothesis of the work for developing a new drug delivery strategy using bacteria-conjugated nanoliposomes (MTB–LP) that can follow a navigation pattern, deeply penetrating tumors by propulsion from the flagella and external magnetic fields controls. A bioconjugation method based on a carbodiimide dehydrating agent[27–29] was developed for the covalent binding of amine containing molecules of bacteria to carboxylated liposomes. The MTB–LP complex was then thoroughly characterized for its structural properties, mobility in directional magnetic field, cellular uptake, and cytotoxicity in relevant cell models in order to demonstrate the feasibility of the proposed strategy for effective target drug delivery.

RESULTS

Characterization of the MTB–LP Complex. The colocalization of TRITC-labeled nanoliposomes with MTB at excitation/emission wavelengths of ~555/580 nm indicate nanoliposome attachment on the surface of MTB and the formation of the complex using confocal laser scanning microscopy (CLSM) (Figure 1a). To further confirm the successful formation of the complex, fluorescence-activated cell sorting (FACS) was performed. The density plots indicate that bare bacteria exhibit a higher forward scatter (FSC) and smaller amount of fluorescence than fluorescent nanoliposomes alone (Figure 1b, left). The MTB–LP plot combines the fluorescence intensity characteristic of nanoliposomes together with the forward scattering characteristics of bacteria cells, distinguished by a broad distribution of fluorescence intensity from that of bare bacteria. Considering that any fluorescent signal exclusively originates from attached liposomes, the percentage of the MTB–LP complex was determined by extracting its fluorescence intensity from controls. The events number and intensity distribution in four quadrants as a percentage of the total of 25 000 events are presented using FlowJo software. It can be concluded that more than 90% of the bacteria were associated with TRITC labeled nanoliposomes and considerable number of liposomes were attached homogeneously to bacteria. These results were also confirmed with the intensity distribution histograms of MTB–LP complexes (Figure 1b, right). Samples were characterized by comparing monomodal fluorescence intensities between each sample. Fluorescent nanoliposomes could clearly be differentiated from bacteria as the latter possess no or minimal background

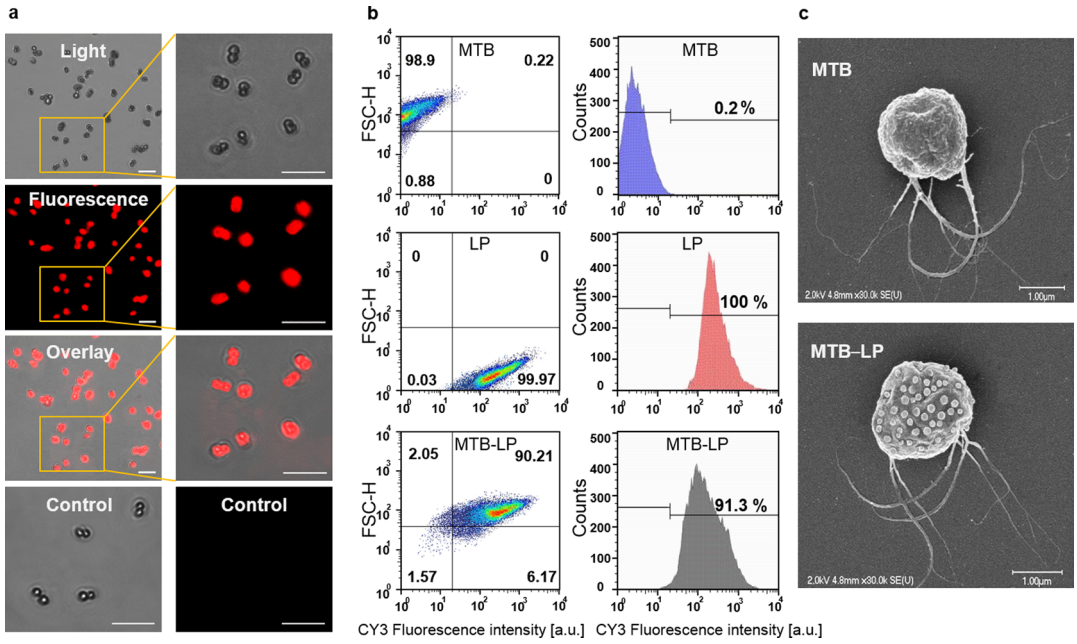

Figure 1. Characterization of nanoliposomes attached to the surface of MC-1 MTB. (a) Confocal microscopy images of TRITC labeled MTB−LP complexes. Photomicrographs show the phase contrast, fluorescence and overlay confocal images. Unlabeled bacteria were used as control. Scale bars show 5 μm at 60× magnification. (b) FACS density plots (left) and histograms (right) obtained from noncoated MC-1 bacteria, TRITC-labeled nanoliposomes, and MTB−LP complex show that bacteria are homogeneously coated with nanoliposomes and can be differentiated from bare bacteria by their fluorescence. Labeling efficacy was determined by dividing the percentage of labeled bacterial cells to total cells. (c) Field emission scanning electron microscopy images of bare MC-1 MTB and MTB−LP complex. The scale bar corresponds to 1 μm. All results are represented as the mean of five independent experiments.

autofluorescence. In addition, the fluorescence intensity distributions of MTB−LP are broader and extend to higher intensities than those observed for bare bacteria indicating the successful bioconjugation between bacteria and nanoliposomes. The relative fluorescence intensity value of the fluorescent liposomes alone was approximately 160-fold higher than that of bacteria cells, while it was only 1.5-fold greater than MTB−LP.

To confirm confocal and FACS analyses and quantify the number of attached nanoliposomes to each bacteria, field-emission scanning transmission electron microscopy (FE-STEM) analysis was carried out. A comparison between SEM images of MTB−LP after multiple washing steps and those of bare MTB confirmed stable attachment of nanoliposomes to the bacterial cell membrane (Figure 1c). The number of attached nanoliposomes to individual bacteria was dependent on concentration and incubation time (Figure 2). For a 1 h incubation time, the number of attached nanoliposomes increased gradually with liposome concentration from 0 to 400 μL of 15 mM liposomes. In the case of 2 h, results demonstrate that this number markedly increases with liposome concentrations from 0 to 100 μL. For a concentration of 4×10^7 MTB cells (10^7 MTB/mL), approximately ~70 ± 5 nanoliposomes could attach when 100 μL of 15 mM liposomes (250 μg mL^{-1}) were used. Further increasing the volume of liposomes up to 400 μL did not improve the efficiency of the attachment and it reached a plateau after a 250 μg mL^{-1} liposomal

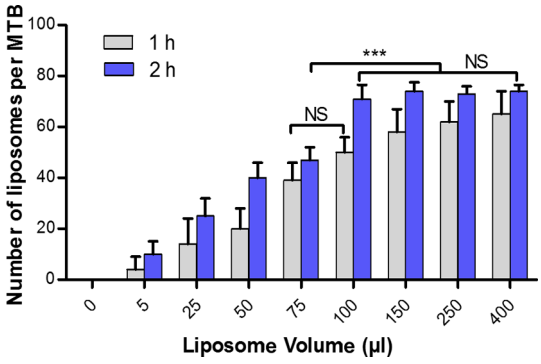

Figure 2. Quantification of the number of nanoliposomes attached to MTB cells by FE-STEM as a function of nanoliposome concentrations in volumes of 0, 5, 25, 50, 75, 100, 150, 250, and 400 μL (15 mM stock solution) for exposure times of 1 and 2 h. The results are presented as the mean number of attached nanoliposomes ± SD, $n = 3$. Results indicate that under 1 h incubation, the number of attached nanoliposomes gradually increases with liposome concentration. While after a 2 h incubation, bacterial surface saturates at volumes exceeding 100 μL. Statistical analysis was performed using two-way ANOVA. *P*-value < 0.001 marked with asterisk (***) is considered significantly different and *P* > 0.05 is not significant (NS).

concentration. This concentration was therefore chosen for all further experiments and analyses.

Monitoring the Magnetic Response and Swimming Behavior of MTB−LP Complex. To ascertain maximum loading of MTB while maintaining maximum velocity after the attachment of the nanoliposomes, the motility functions

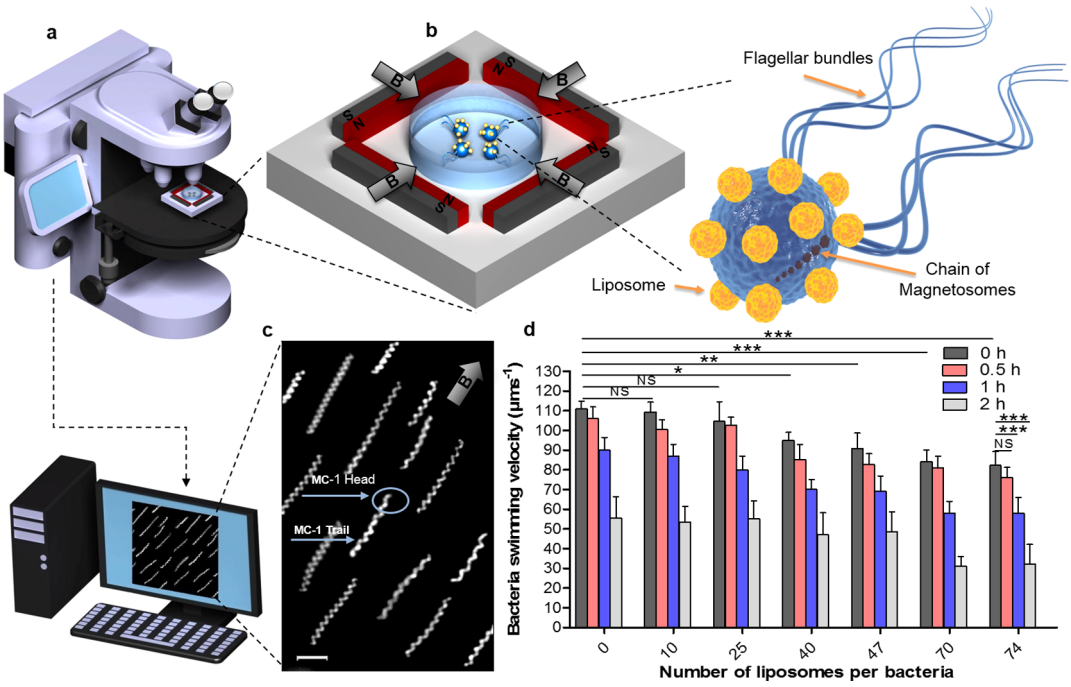

Figure 3. Schematic representation of the experimental setup used to track and visualize MTB−LP complex magnetotactic behavior. (a) Optical microscope. (b) Side view of the two-dimensional magnetic navigational setup including four permanent magnets that generate a homogeneous magnetic field toward the center of the device. Arrows depict the direction of the magnetic field. (c) Motility track of MTB−LP complex under the influence of the magnetic field. Images were recorded by dark field optical microscopy using a 200 ms exposure time for the helical motion in response to 20 G magnetic field. Scale bar indicates 5 μm. (d) The average terminal swimming speeds of loaded and bare MTB (none preselected) *versus* the number of attached nanoliposomes in PBS at room temperature 0, 0.5, 1, and 2 h after washing. Results indicate a decrease of bacterial motility caused by bioconjugation of nanoliposomes to the cell membrane. Data are presented as mean ± SD, $n = 3$. Statistical analysis was performed using two-way ANOVA. Significant difference was considered for *$P < 0.05$, **$P < 0.01$, ***$P < 0.001$ and not significant (NS) for $P > 0.05$.

of MTB−LP such as swimming speed and response to applied magnetic fields were evaluated with a custom-made experimental magnetic component and an optical microscope (Figure 3a,b). The magnetic setup was composed of four permanent magnets facing each other two by two to generate a homogeneous two-dimensional magnetic gradient (Figure 3b). The magnetic gradient field direction was oriented toward the center with gradually decreasing magnitude to 0 G at the center. The magnet setup was placed under an optical microscope, and observation was carried out at the specific position where a directional magnetic field of approximately 20 G resulted in straight swimming paths of the bacteria.

The helical motion and trail left of the MTB could therefore be evaluated by decreasing the shutter speed of the camera to 200 ms (Figure 3c). Results show that the terminal swimming velocity of MTB−LP complexes is dependent on the number of nanoliposomes attached to bacteria, since the increased number of attached nanoliposomes reduces the motility (Figure 3d). MTB−LP complexes carrying up to approximately 70 liposomes responded to a similar magnitude of the magnetic field as compared to bare bacteria prepared and tested in the same conditions. At early time points *i.e.*, 30 min, the terminal velocity of these highly loaded complexes could reach around 80 μm s^{-1}. Results also indicate that the residency time of MTB−LP complexes in PBS has a major impact on the mobility of the bacteria. Long incubation times (more than 2 h) in buffer solution significantly decrease the motility of both MTB−LP and bare bacteria (Figure 3d). The motility of MTB−LP complexes with 70 nanoliposomes dropped to 32 μm s^{-1} after 2 h suggesting that the complex should be used for self-propelled target delivery purposes within 30 min of the preparation.

Biological Characterization of MTB−LP Complex. Cell viability graphs are presented for different concentrations of MTB−LP complexes at different incubation times (3, 6, 12, 24, and 48 h) using WST-1 assay (Figure 4). The viability of all tested cell lines (NIH/3T3, J774, and Colo205) were time, MTB−LP, and MTB bacteria dose dependent. Maximum cytotoxic levels were observed at highest bacterial concentration (10^8 MTB/well) after 48 h of incubation. No significant cell viability reduction could be observed between 24 and 48 h exposure times for NIH/3T3 and J774 (Figure 4a,b,d,e). Interestingly, the viability of MTB−LP was similar to bare nanoliposomes for Colo205 at MTB concentrations ranging from 2×10^5 to 6×10^6 (Figure 4h,i). In contrast, Colo205 cells demonstrated a significant increase in cytotoxicity for concentrations ranging from 6×10^6 to 10^8 MTB/well for both MTB−LP complex and bare MTB (Figure 4g,h).

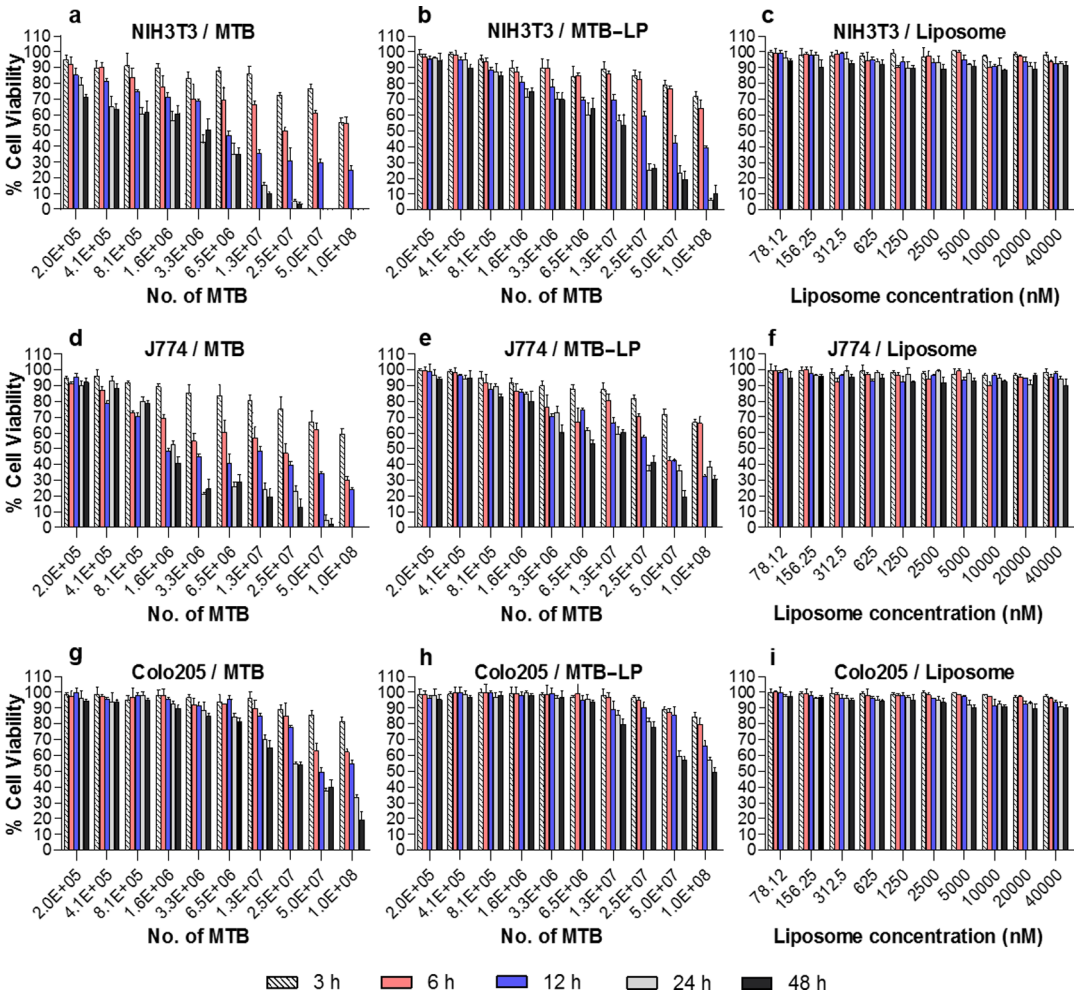

Figure 4. Inhibitory effects of MTB formulation on viability of tested cell lines. Effect of incubation time and concentration of MTB−LP complex on viability of NIH/3T3 (a−c), J774 (d−f), and Colo205 (g−i) cell lines as compared to bare MTB and bare nanoliposomes using the WST-1 assay. Cells were incubated for 3, 6, 12, 24, and 48 h at 37 °C with 2×10^5 to 10^8 (MTB/well) for MTB/MTB−LP and 0.07−40 μM for bare nanoliposomes. Viability responses were found to be cell-type, dose, and time dependent. While the results show that cells survive long after exposure to bare nanoliposomes, the bacterial formulations reduced viability of the tested cell lines. Cancer cells were shown to be less vulnerable than normal cells. Results demonstrate that cell viability was greater for MTB−LP compared to bare MTB. Data were normalized to untreated cell lines (controls). Error bars, mean ± SD, $n = 4$.

The MTB−LP exhibited a less cytotoxic effect on tested cell types at all concentrations compared to bare MTB (approximately 20−40%) indicating that the cell viability was improved through the attachment of nanoliposomes on the surface of bacteria. The free nanoliposomes in the experimental range of 0.07−40 μM did not induce significant cytotoxicity on tested cell types (Figure 4c,f,i).

The comparison of half maximal inhibitory concentration (IC_{50}) values for MTB and MTB−LP in three tested cell lines indicates that a lower incubation time requires higher concentrations to reach the IC_{50} (Table 1). The rank order of IC_{50} associated with bare MTB and MTB−LP cytotoxicity was as follows: Colo205 > J774 > NIH/3T3. In addition, results reveal that the cytotoxicity is reduced when the biocompatible nanoliposomal moieties are attached to the bacteria. In this case, higher concentrations of MTB−LP complexes are needed to reach the 50% cell survival rates compared to bare MTB.

Incubation of fluorescent MTB−LP complexes with the cell lines and subsequent observation by confocal microscopy shows localization of complexes mainly in the cytoplasm and perinuclear region (Figure 5a). The same localization was also found for fluorescence bare liposomes used as control (Supporting Information Figure S2). Overall, the samples internalized and migrated in a time-dependent manner toward the nucleus of cells but did not enter the nucleus. Z-stack confocal images reconstructed using Imaris image analysis software (Bitplane AG) confirm that complexes are indeed internalized by the cells and not simply bound to their surface (data not shown). CellProfiler image analysis software was used to quantify the fluorescence signal intensity of uptaken nanoliposome alone and complexed. To derive an accurate quantification, the ratio of fluorescence intensity of internalized liposomes or MTB−LP relative to cell nuclei was

TABLE 1. IC_{50} Values of the MTB and MTB−LP for the Tested Cell Lines[a]

		incubation time				
cell type	samples	3 h	6 h	12 h	24 h	48 h
NIH/3T3 Fibroblast	MTB- LP	1.255×10^7	1.042×10^7	9.779×10^6	6.286×10^6	9.076×10^5
	MTB	3.289×10^6	3.149×10^6	1.980×10^6	1.172×10^6	7.179×10^5
J774 Macrophage	MTB- LP	4.838×10^7	2.727×10^7	1.506×10^7	9.639×10^6	6.720×10^6
	MTB	8.244×10^6	7.050×10^6	4.533×10^6	2.722×10^6	9.175×10^5
Colo205 Cancer cells	MTB- LP	1.945×10^8	1.784×10^8	8.164×10^7	4.047×10^7	1.284×10^7
	MTB	9.721×10^7	8.052×10^7	4.219×10^7	2.930×10^7	8.321×10^6

[a] Data are presented as the numbers of MTB in each well. MTB has growth-suppressive effects comparable with those of MTB—LP in tested cell lines. Data were normalized to untreated cell lines (controls) $n = 3$.

calculated. As shown in Figure 5b, the MTB−LP uptake is cell-type dependent. J774 cells as a photogenic cell model display the highest uptake capabilities for both free nanoliposomes and MTB−LP complexes compared to the two other nonphagocytic cells. Fluorescence signal related to MTB−LP uptake slightly increased in nonphagocytic cell lines after a 6 h incubation.

Moreover, the complex exhibits significantly enhanced translocation into the J774 and NIH/3T3 cells as compared to Colo205 cancer cells. Interestingly, although free liposomes could generally be internalized faster relative to MTB−LP in nonphagocyte cells, the level of uptake is higher for the complex than for bare nanoliposomes, particularly by J774 cells. The fluorescent signal intensity increased gradually until 12 h incubation in J774 and NIH/3T3 cells and then reached a plateau suggesting that cells has reached their saturation capacity, while accumulation continued in cancer cells and significant uptake improvement was measured when the incubation time was extended to 24 h.

DISCUSSION

Despite advancements in targeted drug delivery, many relevant diagnostic and therapeutic products, including local and systemic administration by ligand-drug-conjugates[4,30] or Magnetic Drug Targeting (MDT),[31,32] have not been entirely effective, and clinical trials are still forthcoming. Various methods of MDT have investigated the applicability of superparamagnetic iron oxides (SPION)[32] and Fe−Co nanoparticles,[1] as well as magnetosomes isolated from MTB[27,33] for MRI imaging, targeting, and drug delivery.[32,34] To date, however, concerns regarding poor pharmacokinetic profiles, force limitations of small magnetic carriers in complex microvascular networks,[35] lack of navigation to organs located deep in the body,[18] poor depth penetration, and cytotoxicity remain barriers to clinical entry. The proposed MTB−LP complex combines several novel aspects that can overcome many of the aforementioned limitations relative to traditional polymeric and magneto-based platforms and render the system as a viable vehicle for target drug delivery. The proposed route of injection for MTB−LP would be peritumoral (PT) injections for solid tumors that are accessible (*e.g.*, colorectal, prostatic, *etc.*), to avoid the vasculature where the blood flow (ranging from a few tens of centimeters per second)[36] could carry the agents away from the intended target. For PT-based interventions, drug-loaded MTB can be directly injected in the vicinity of the tumor and as close as possible to the angiogenic microenvironment without touching the tumor mass to take advantage of the directional blood flow toward the tumor with minimal flow rate and to reduce the risk of systemic toxicity.

Bioconjugation was performed using a carbodiimide dehydrating agent[27−29] by taking advantage of terminal amine groups on the outer membrane of bacteria that are ideal docking sites for amide covalent attachment of carboxylated nanoliposomes to MTB cells. These functional amine groups are present as parts of organized phospholipids, lipopolysaccharides (LPS), lipoproteins and surface proteins assemblies such as lysine, D-alanine, or polypeptides.[37,38] Carbodiimide cross-linking is a versatile technique used to prepare biomolecular probes, conjugate antibodies, peptides, proteins, *etc.* onto nano/microparticle,[39,40] and immobilize macromolecules for use in numerous applications,[41] demonstrating a stable chemical bond for *in vitro* and *in vivo* applications. The merits of the carbodiimide technique include the ease of sample preparation, high coupling efficiencies, reproducibility, reduced cost, and, most importantly, high strength bond. It should be noted that the enthalpies ($\Delta H°_{298}$) for amide bond formation using carbodiimide chemistry and bond dissociation enthalpies range from 375−422 and 305−440 kJmol^{-1}, respectively.[42] The dissociation energy is much higher compared to other methods such as antibody−antigen affinity type bioconjugation including van der Waals forces, electrostatic forces, hydrogen bonds, and hydrophobic effects, which range from 4 to 30 kJ mol^{-1}.[43] Therefore, the covalent amide bonds are much stronger than affinity-based antibody conjugation and require considerable energy to break. It is robust in an *in vivo* environment and also compatible with MTB compared to other bioconjugation techniques. For instance, passive

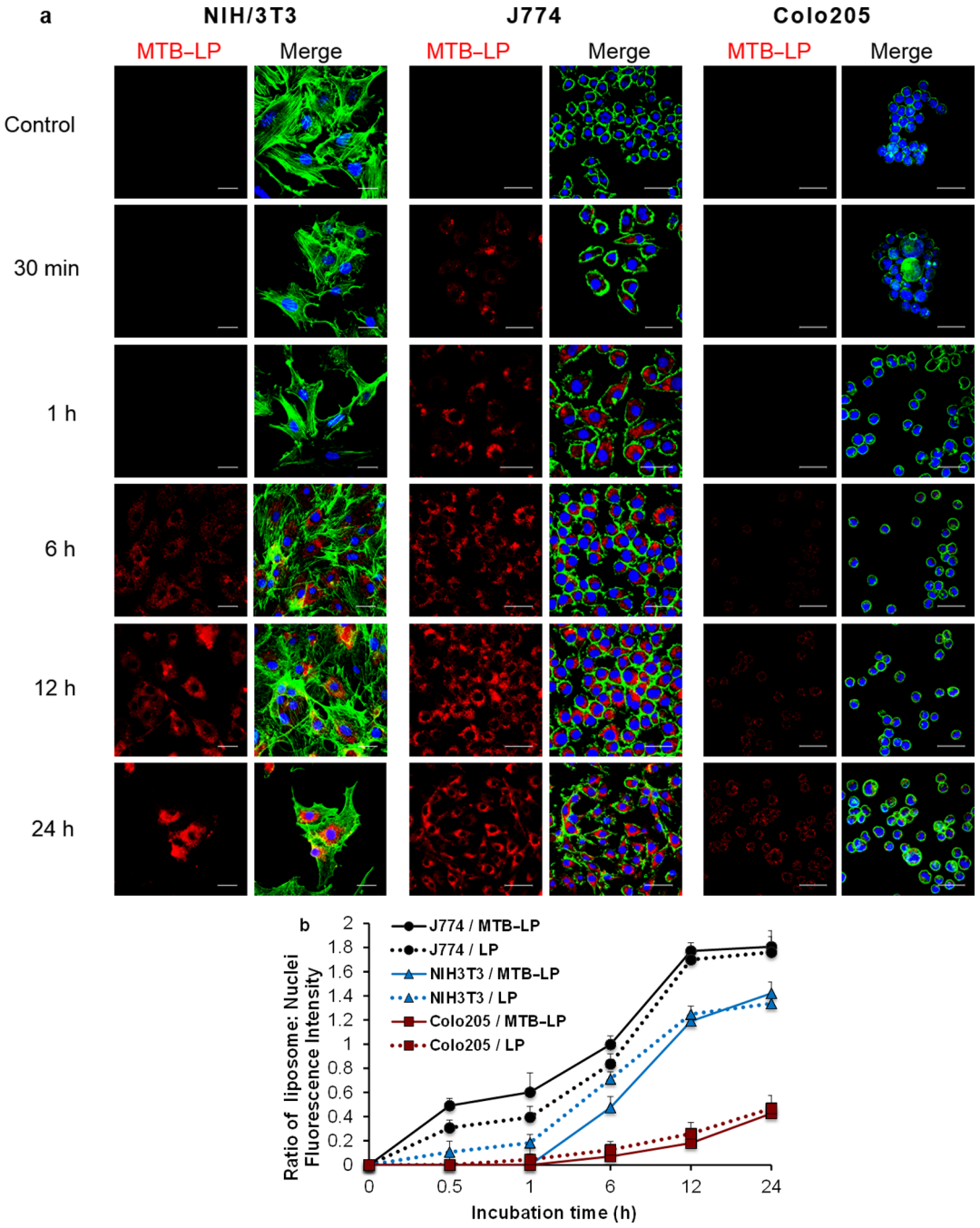

Figure 5. (a) Confocal microscopy images of time-dependent MTB−LP complex uptake by J774, NIH/3T3, and Colo205 cell lines at different incubation times. Fluorescently labeled nanoliposomes exhibit a very strong fluorescent signal. Actin filaments were visualized with Alexa Fluor 488 Phalloidin (green) and nuclei were stained with Hoechst 33342 (blue). The pictures were taken at the midsection of the cells. Bar indicates 30 μm. (b) The values reported are obtained by dividing the fluorescence intensity of bare liposomes or MTB−LP by that of nuclei in each fluorescence image over time. Values represent mean $\pm$ SD, n = 3.

adsorption through electrostatic or van der Waals type attractions[44] suffers from poor stability for *in vivo* applications. Noncovalent affinity based bonds such as biotin−avidin[45] rely on manipulation of both bacteria and liposomes, which cause treated MTB to lose their functionality and viability due to the treatment processes and excessive use of chemical reagents. Antibody conjugation[46] for immunoliposome[47] preparation also has major drawbacks, specifically the cost involved in custom antibody production, especially for monoclonal antibodies. The lack of specificity of polyclonal antibodies could result in targeting both the bacterial head and flagella, which can negatively affect the velocity and straight motility of the bacteria.

In physiological conditions, amide bonds are not affected by medium conditions such as pH or ions and

are quite resilient to imposed mechanical forces. Moreover, hydrolysis and enzymatic cleavage (by serum proteins/cellular secreted products) of amide bonds is highly dependent on the microenvironment condition and exposure time.[48] Considering that the bacteria can only survive for 40 min at body temperature due to their nonpathogenic nature,[19] the *in vivo* navigation would be performed in under 30 min, in which the covalent bonds would likely remain stable. This bioconjugation technique provides a one size fits all approach matching the experimental conditions required for the MTB cell bioconjugation.

Results from SEM, FACS, and confocal microscopy (Figure 1) reveal that the exogenous nanoliposomes are firmly linked to MTB cell membranes and remain on the bacterial cell surface, even after harsh washing conditions. Interestingly, as it can be observed on SEM images, most liposomes were localized on MTB main body, while a negligible number (less than 2%) were attached to the flagella. Optimizing the number of liposomes per bacteria was a key challenge in the development of the complex to carry sufficient concentrations of drug to exert therapeutic effects without compromising natural bacteria motility. Considering the surface area of a typical MTB ($\sim$1.5 μm in diameter), we found that coupling of up to 70 nanoliposomes with an average size of 170 nm to the surface of bacterial cells occludes only about 23% of the total cell surface without significantly altering MTB–LP mobility and responsiveness to the applied magnetic field.

Indeed, the swimming speed of the complexes only decreased by approximately 27% (from 110 down to approximately 80 μm s^{-1}) when $\sim$70 liposomes are attached to the surface (Figure 3d). However, it should be noted that the terminal velocity of MTB–LP was still higher than that of typical morphotypes of magnetotactic bacteria such as AMB-1 (49 μm s^{-1}), MS-1 (40 μm s^{-1}), *etc.*, at the same magnitude of applied magnetic field[18] even after the bioconjugation process, weight of nanoliposomes, long-term exposure to PBS, and multiple turnovers of the culture environment. Moreover, the velocity of MTB–LP was greater than the linear swimming speed of some other nonmagnetotactic flagellated bacteria strains such as *Salmonella* (20–50 μm s^{-1}) or *E. coli* (10–40 μm s^{-1}), which can overcome diffusion resistances in solid tumors with this range of velocities.[15,16]

The uptake and internalization behaviors of free/attached liposomes were compared to those exhibited by macrophage, fibroblast, and colorectal cancer cells to assess whether tumor and nontumor cells exploit various uptake dynamics. The results show that the MTB–LP complex was rapidly internalized by J774 phagocytic cells, whereas the opposite was observed for nonphagocytic cells (NIH/3T3 and Colo205) (Figure 5; Supporting Information Figure S2). Moreover, the level of uptake of negatively charged liposomes and MTB–LP in cancer cells (Colo205) was lower than that in normal cells (NIH/3T3, J774). As reported in the literature, cell phenotype (cancerous *vs* normal cells),[49,50] the cell's endocytic capacity (phagocytosis *vs* nonphagocytosis),[51] bacteria type (pathogenic *vs* nonpathogenic),[52,53] and attachment bond, as well as liposomal size[54] and surface charge,[51] determine the mode and capacity of cellular uptake.

Negatively charged liposomes are believed to enter cells *via* nonspecific receptors present on a variety of cells, which in turn mediate particle recognition, adhesion, and the subsequent endocytotic-like internalization mechanisms.[51,55] Conversely, cancer cell membranes possess an enhanced net negative surface charge compared to normal cells as a result of extensive sialylation,[50] abundance of phosphatidylserine residues, heparan sulfate proteoglycans, and *O*-sialoglycoproteins.[56] This may lead to repulsion of negatively charged nanoparticles or complexes and reduced cellular uptake. Accordingly, the low MTB–LP uptake by Colo205 cell line can be explained by the presence of negatively charged nanoliposomes.

Bacteria, in their turn, exploit different pathways for cellular uptake, including phagocytosis or pinocytosis. However, the uptake process of both pathogenic and nonpathogenic bacteria in epithelial cells or fibroblasts, representing classical nonphagocytic cells, is through nonselective internalization mechanisms, such as macropinocytosis,[52,53] which depend on external stimuli to trigger a signaling cascade. Only metabolically active bacteria can undergo this process since heat-treated bacteria did not induce any fluid-phase uptake.[52,53] In our case, MTB bacteria are affected by mammalian cell culture conditions, mainly the 37 °C temperature. At this temperature, they cannot proliferate and remain active only for 30–40 min.[19] Therefore, we cannot conclude that MTB take advantage of macropinocytosis. Future studies will investigate whether nanoliposomes undergo detachment from bacteria in the cellular environment or if MTB–LP complexes themselves can be internalized by nonphagocytic cells. The particular mechanisms involved in the entry of MTB into nonphagocytic cells remain to be elucidated. However, the lack of fluorescence signal from complexes at the initial incubation time indicates that liposomes should remain attached to the bacterial surface, and regardless of the underlying internalization mechanism, nanoliposomes containing therapeutic agents could enter the cell effectively for intracellular drug delivery applications.

Cell viability assays also support that MTB–LP show higher cell viability than MTB (Figure 4 and Table 1) due to the incorporation of biocompatible nanoliposomes.[57] Nonetheless, it is important to note that substances produced by the bacteria, certain degradation products, or competition for nutrients in the *in vitro* environment may also affect cell viability and result in concentration

dependent cytotoxicity. Ultimately, benign concentrations of bacteria should be determined for *in vivo* assays, high enough to deliver sufficient therapeutic payload but lower than the cytotoxicity threshold.

CONCLUSION

We developed a new-generation of therapeutic vector by introducing a direct, reproducible, and clinically applicable chemical coupling of carboxylated nanoliposomes to pre-existing reactive groups naturally present on the surface of transporter MC-1 MTB *via* carbodiimide cross-linking chemistry. This bioconjugation strategy and the number of attached liposomes do not alter intrinsic bacterial motility and their behavior under a controlled magnetic field. The attachment of nanoliposomes improves the cellular viability of the complexes and does not interfere with their uptake. Through the combination of their suitable magneto-aerotaxis behavior, improved systemic biocompatibility, native bacteria cytotoxicity at tumor sites, therapeutic or diagnostic agents transport, and cellular uptake, this engineered MTB–LP system offers opportunity for their application in cellular tracking, medical imaging, and the ability to actively target areas of interest while increasing the maximum-tolerated dose of pharmacytes for cancer therapy, gene or vaccine delivery. Taking into account the encapsulation efficacy of drug within liposomes, the average number of liposomes carried by each bacteria, and the number of injected bacteria, it is possible to estimate the deliverable dosage of drug that will be released at the tumor site. Our system can potentially overcome targeting and diffusion limits by actively penetrating hypoxic regions of tumors currently unattainable with conventional cancer drugs and effectively deliver active substances to solid tumors.

METHODS

Reagents and Chemicals. The lipids distearoylphosphatidylcholine (DSPC), distearoylphosphatidylethanolamine derivatives of PEG with a terminal carboxyl group (DSPE-PEG2000-COOH) were purchased from Avanti Polar Lipids, Inc. (Alabaster, AL). Cholesterol, *N*-hydroxysulfosuccinimide (sulfo-NHS), 1-ethyl-3-[3-(dimethylamino)propyl]-carbodiimide (EDC), 2-(*N*-morpholino)-ethanesulfonic acid (MES), sepharose CL-4B, glutaraldehyde, trypsin–EDTA solution, and phosphate-buffered saline (PBS) were all acquired from Sigma-Aldrich (St. Louis, MO). Poly-L-lysine was purchased from Electron Microscopy Sciences, Inc. Rare earth magnets were purchased from Indigo Instruments (Waterloo, Canada). *N*-(6-Tetramethylrhodaminethiocarbamoyl)-1,2-dihexadecanoyl-*sn*-glycero-3-phosphoethanolamine, triethylammonium salt (TRITC DHPE), lissamine rhodamine B 1, 2-dihexadecanoyl-*sn*-glycero-3-phosphoethanolamine, triethylammonium salt (rhodamine DHPE), penicillin–streptomycin, bovine calf serum (BCS), and fetal bovine serum (FBS) were obtained from Invitrogen (Burlington, CA). NIH/3T3 (ATCC CRL-1658) mouse embryonic fibroblast cells, J774A.1 (ATCC TIB-67) murine macrophage cell lines, Colo205 (ATCC CCL-222) human colorectal adenocarcinoma cell line, Dulbecco's Modified Eagle's Medium (DMEM) (ATCC30-2002) and Roswell Park Memorial Institute 1640 medium (RPMI-1640) were purchased from American Type Culture Collection (Manassas, VA). 4-[3-(4-Iodophenyl)-2-(4-nitrophenyl)-2*H*-5-tetrazolio]-1,3-benzene disulfonate (WST-1) was purchased from BioVision, Inc. A Milli-Q water system (Millipore, Bedford, MA), supplied with distilled water, provided high purity water (18 MΩ) for these experiments.

Culture Growth Conditions for MC-1 Magnetotactic Strain. *Magnetococcus marinus* MC-1 strain from our laboratory stock was cultured microaerobically in chemoheterolithotrophic medium at room temperature, as previously reported.[58] Bacterial cultures were incubated statically under an oxygen concentration gradient ($[O_2]$-gradient) in an iron enrichment medium, which included 50 μM ferrous sulfate, $FeSO_4 \cdot 7H_2O$ (Sigma-Aldrich), to allow the biomineralization of magnetic nanoparticles. The MC-1 culture was incubated for 48 h without agitation at 25 °C in the dark. Bacterial cells were harvested during the stationary phase of growth and used for direct observation or conjugation with liposomes in this study.

Fabrication and Characterization of Nanoliposomes. See Supporting Information.

Covalent Coupling of Carboxylated Nanoliposomes to MTB Cells Using Carbodiimide Chemistry. To stably couple nanoliposomes to the surface of magnetotactic bacteria cells, we exploited the fact that many cells have high levels of intrinsic amine groups on their surfaces. The most straightforward approach to immobilize and maintain functionalized liposomes with reactive carboxylic acid groups (–COOH) in the range of 170 nm to the surface of bacteria was to use direct covalent chemical conjugation. To avoid loss of bacteria viability, conventional bioconjugation methods based on zero-length carbodiimide chemistry (EDC/NHS) were carefully adapted as a robust and highly versatile methodology for introducing functional surface of component to cell membrane.[29]

The MTB–LP complex was achieved by a two-step process (Supporting Information Scheme S1). First, the carboxylated nanoliposomes were activated using EDC/NHS chemistry by incubating 100 μL of a liposome solution (stock liposome solution; 15 mM) with the carbodiimide activating reagents EDC and sulfo-NHS (EDC/NHS/DSPE-PEG-COOH = 30:30:3, mol/mol) for 20 min in MES buffer (pH = 5.5) at room temperature. A Sepharose CL-4B column was used to remove the excess activating reagents. The carbodiimide-based coupling reagent can react with the carboxylic acid groups of liposomes to provide a highly active ester (*O*-acylisourea) intermediate that could then react with a nucleophile, such as a primary amine, to form an amide bond[29] (Supporting Information Scheme S1). Subsequently, bioconjugation was achieved by incubating approximately 4×10^7 ($\sim 10^7$ MTB/mL) MTB bacteria cells with activated nanoliposomes. The mixture was then incubated for 1 or 2 h at 25 °C under gentle agitation to permit amide coupling. Attached liposomes were separated from unbound liposomes using a two-dimensional magnetic field (Figure 3b) followed by three rinses with PBS. The sample was redispersed in PBS at pH 7.4. To develop an optimal protocol for MTB–LP complexes and determine the maximum capacity for carrying liposomes, different liposome concentrations ranging from 0, 5, 25, 50, 75, 100, 150, 250, and 400 μL (15 mM) were added to an equal quantity of bacteria (4 mL of 10^7 MTB/mL) and incubated for 1 and 2 h at 25 °C with gentle mixing.

Assessment of Nanoparticle Attachment to MC-1 MTB Bacteria. Construction and attachment efficacy of MTB–LP complexes were examined using confocal laser scanning microscopy (CLSM), scanning electron microscopy (SEM) and fluorescence activated cell sorting (FACS) flow cytometry techniques. All the experiments were performed in triplicate in order to ensure consistency and reproducibility through statistical significance.

Fluorescence signals from MTB–LP were acquired using confocal laser scanning microscopy (CLSM: Carl Zeiss LSM 510-META with Axiovert inverted microscope, Jena, Germany). TRITC labeled liposomes were visualized with a He/Ne laser (543 nm excitation and a 560–615 nm band-pass emission filter), while scattered incident light was simultaneously

observed *via* the transmitted light detector. Images were obtained through a high numerical aperture (NA) 63.0 × 1.4 oil-immersion objective and Carl Zeiss LSM imaging software.

In addition, fluorescence and scattering intensity distributions of bacteria treated with nanoliposomes were measured by TRITC tagged lipids using fluorescence activated cell sorting analysis (FACS: BD FACSCalibur; BD Biosciences) with a laser excitation wavelength of 543 nm. Samples were diluted 1 in 10 in PBS and the measurement was carried out using forward scatter *versus* fluorescence (FSC/FL1) plots for 25 000 events. Bare bacteria were used as a control. FACS data was analyzed by FlowJo software (Tree Star, Inc., Ashland, OR), using appropriate gates and controls to generate density plots and histograms of each sample.

The number of liposomes attached to the MTB surface was assessed by FE-STEM. After each incubation time point, a suspension of MTB−LP was fixed with 3% glutaraldehyde (Sigma-Aldrich, Oakville, Ontario) in 0.12 M PBS (pH 7.2) at 4 °C. A suspension of fixed samples (20 μL) was placed onto a poly-L-lysine coated 12 mm glass slide and incubated for 30 min. The slides were then rinsed with ultrapure water. Samples were dehydrated in a series of ethanol/water solutions of increasing ethanol content from 30% to 100%. Dehydration was followed by critical point drying to remove ethanol from the sample (Leica Microsystems Critical Point Dryer Model CPD030). Samples were finally mounted on carbon tape and wafer sputtered with gold/palladium prior to imaging (Anatech Hummer VI sputtering coater, Arlington, VA). High-resolution images were obtained using a Hitachi S-4700 FE-STEM at an accelerating voltage from 2 to 5 kV, an emission current of 15 μm and working distances of <5.3 mm. To determine the average number of attached liposomes to the surface, their number was counted on 100 bacterial cells at each concentration.

Investigation of Magnetotaxis Behavior of MTB−LP Complexes by Optical Microscopy. The swimming velocity and magnetotaxis-based behavior of MTB−LP complexes at different number of attached liposomes per MTB (0, 10, 25, 40, 47, 70 and 74) after 0, 0.5, 1, and 2 h sample preparation were examined using a phase contrast microscope (AxioImager Z1, Imaging Solutions Carl ZEISS) with a resolution of 1388 × 1040 pixels and a dynamic range of 12-bits. Images were acquired by AxioCamMRm CCD camera (Zeiss) bearing a long distance objective Ediplan 50×, dark-field illumination in reflection-mode while applying 20 G external magnetic field. A gaussmeter probe (model 450, Lake Shore Cryotronics, Inc.) was used to quantify the magnetic field at this position. To obtain consistent results, the exposure time of the camera was set to 200 ms, allowing the visualization of the trail left by bacterial motion. All measurements were made using AxioVision v.4.6.0 software. As mentioned earlier, the initial swimming velocity of unloaded MC-1 bacteria in complete growth medium at room temperature can exceed 200 μm s^{-1}. However, bare MTB bacteria, washed three times in PBS-1× (pH = 7.4), showed velocity decrease to about 110 μm s^{-1} using 2D magnetic field. This was set as a reference velocity to compare the swimming speed of bare MTB and MTB−LP complexes from ∼500 non-preselected bacteria images.

Evaluation of Cellular Toxicity and Uptake. *Cell Culture.* The Colo205 was cultured in RPMI-1640 medium. J774A.1 and NIH/3T3 were grown in DMEM under recommended conditions. NIH/3T3 cells were supplemented with 10% BCS and 1% penicillin/streptomycin. Colo205 and J774A.1 cell lines were supplemented with 10% FBS and 1% penicillin/streptomycin. All cells were cultured in an atmosphere of 5% CO_2 at 37 °C in a fully humidified incubator. NIH/3T3 and Colo205 cells were harvested using commercial trypsin (0.05% trypsin-EDTA; Gibco). J774.A cells were scraped and viable cell concentrations were determined by 0.4% Trypan blue staining.

WST-1 Based Cell Inhibition and Cytotoxicity Assays. The growth inhibitory effect of the MTB−LP complex was evaluated with a WST-1 colorimetric assay.[59] MTB alone and blank liposomes were used as control. First, J774, Colo205, and NIH/3T3 cells were seeded in growth medium at a density of 1 × 10^5 cells/well into 96-well flat bottom plates (Costar, Corning, NY) in triplicates and incubated overnight to allow adhesion to plates. Nonadherent cells were removed by washing with media just before addition of the MTB−LP complex. Incubation time and concentration were considered as effective variables to determine cytotoxicity. Cytotoxicity on a panel of tumor and nontumor cells was determined by exposing cells to serial dilutions of liposomes (0.07−40 μM), MTB−LP (2 × 10^5 to 10^8; 0.022−11.6 μM ((MTB/well); liposome) and MTB (2 × 10^5 to 10^8 MTB/well) from the stock in the appropriate growth medium (without penicillin). Cells were treated with the formulations for variable time periods 3, 6, 12, 24, and 48 h and incubated in a humidified incubator. Then, a WST-1 cytotoxicity assay (G-Biosciences) was performed according to the manufacturer's instructions. Briefly, after the planned incubation time, 10 μL of cell viability proliferation reagent WST-1 (1:10 dilution) was added to each well and the sample was incubated for an additional 2 h at 37 °C under 5% CO_2. Absorbance of formazan dye produced by viable cells was then measured in a microplate reader (Biotek μQuant Monochromatic Microplate Spectrophometer) at 450 nm with a reference wavelength of 620 nm. Wells with cells alone (without bacteria and/or liposome) served as controls to determine the percentage of cytotoxicity in bacterial infected wells. The same amounts of culture medium and WST-1 reagent in empty wells were also included in every experiment as a blank control. The WST-1 reagent incubation time of 2 h was found to be optimum since the color intensity did not change after 2 h (data not shown), and this condition was used in all subsequent assays. Three independent experiments were performed, each in triplicate and viability values were expressed as a percentage of control and plotted *versus* concentration. Cell viability was calculated with respect to cells as control. A sigmoidal dose−response curve was fitted to the data and a half maximal inhibitory concentration (IC_{50}) value was calculated for each replicate, using GraphPad Prism software (version 6.0).

In Vitro Cell Uptake Study. To visualize and determine cellular uptake, the liposomes were fluorescently labeled by incorporating 1 mol % rhodamine-DHPE (head groups marker) into the original formulation with excitation/emission maxima ∼560/580 nm. To study the effect of attachment on the liposomal uptake, all viable cell lines were seeded in complete growth medium at a density of 1 × 10^4 cells/well in a poly-L-lysine coated 35 mm confocal glass bottom Petri dishes with a 14 mm cover glass center (Mattek Corp.). Cells were incubated overnight at 37 °C under 5% CO_2 in a humidified incubator to allow for uniform cell attachment. Following incubation, the medium was then aspirated from the wells and replaced with the stock liposome suspension (200 nM) or MTB−LP complex (10^6 MTB/Petri) in complete growth medium (without penicillin). The quantity of MTB−LP samples for the uptake study was selected based on the lowest IC_{50} concentration measured among all three cell lines after 24 h incubation. Moreover, liposomes alone were used as control with the same concentration as attached liposomes to MTB. Cells incubated with plain growth medium served as controls. The cells and samples were then incubated for different time intervals (0.5, 1, 6, 12, and 24 h) to allow for sufficient uptake.

Assessment of Cellular Uptake by Confocal Imaging. Confocal microscopy on each cell monolayer from randomly selected areas was performed to investigate the internalization and intracellular distribution of the MTB−LP complex and liposomes alone. Following incubation of cells with each formulation, the medium was aspirated and cells were washed three times with cold phosphate buffered saline (PBS) to eliminate traces of liposomes and bacteria left in the wells. Cells were fixed with 10% formalin (Sigma-Aldrich, Oakville, Ontario) for 20 min and washed another three times with PBS. Cells were then permeabilized with 0.1% Triton-X (Invitrogen, Carlsbad, CA) for 5 min and stained with Hoechst 33342 (Molecular Probes, Eugene, OR) and Alexa-488 conjugated Phalloidin (Molecular Probes R, Invitrogen) for nuclei and F-actin visualization, respectively. The cell-containing cover glass at the center of the confocal glass bottom dishes was then mounted with Clear-Mount mounting solution (Invitrogen, Carlsbad, CA).

Microscopic observation of the fluorescent probes delivered to cells was performed with the previously mentioned confocal laser-scanning microscope. All images were acquired while

maintaining a constant laser intensity and detector gain. Following image acquisition, the composite images were assembled using ImageJ (MacBiophotonics) software (NIH, Bethesda, MD). The intensity of fluorescence was evaluated for uptaken liposomes and cell nuclei using CellProfiler image analysis software (Broad Institute, Cambridge, MA). The ratio of fluorescence intensity of uptaken vesicles relative to cell nuclei was then determined to give a quantitative analysis of cellular uptake.

Statistical Analysis. Quantitative data are expressed as a mean ± standard deviation (SD) and the number of independent replicates is indicated in the figure legends. Statistical significance was evaluated with the use of a one- or two-way ANOVA as appropriate followed by a post-hoc Bonferroni test to compare individual means using GraphPad Prism version 6.0 software. The level of statistically significance was set at *P*-values of 0.05 or less for all of the tests.

Conflict of Interest: The authors declare no competing financial interest.

Acknowledgment. This project is funded by the Quebec Consortium for Drug Discovery (CQDM) and in part by a Discover Grant from the Natural Sciences and Engineering Research Council of Canada (NSERC), Mathematics of Information Technology and Complex Systems (MITACS) and the Research Chair of École Polytechnique in NanoRobotics.

Supporting Information Available: Physicochemical characterization of nanoliposomes, carbodiimide-based conjugation of the nanoliposomes to MTB cells, and confocal images of NIH/3T3, Colo205 and J774 cells showing uptake of rhodamine labeled nanoliposomes. This material is available free of charge *via* the Internet at http://pubs.acs.org.

REFERENCES AND NOTES

1. Pouponneau, P.; Leroux, J. C.; Soulez, G.; Gaboury, L.; Martel, S. Co-Encapsulation of Magnetic Nanoparticles and Doxorubicin into Biodegradable Microcarriers for Deep Tissue Targeting by Vascular MRI Navigation. *Biomaterials* **2011**, *32*, 3481–3486.
2. Al-Jamal, W. T.; Kostarelos, K. Liposomes: From a Clinically Established Drug Delivery System to a Nanoparticle Platform for Theranostic Nanomedicine. *Acc. Chem. Res.* **2011**, *44*, 1094–1104.
3. Mikhaylov, G.; Mikac, U.; Magaeva, A. A.; Itin, V. I.; Naiden, E. P.; Psakhye, I.; Babes, L.; Reinheckel, T.; Peters, C.; Zeiser, R.; *et al.* Ferri-Liposomes as an MRI-Visible Drug-Delivery System for Targeting Tumours and Their Microenvironment. *Nat. Nanotechnol.* **2011**, *6*, 594–602.
4. Torchilin, V. P. Passive and Active Drug Targeting: Drug Delivery to Tumors as an Example. In *Handbook of Experimental Pharmacology*; Hofmann, F. B., Ed.; Springer: New York, 2010; pp 3−53.
5. Brannon-Peppas, L.; Blanchette, J. O. Nanoparticle and Targeted Systems for Cancer Therapy. *Adv. Drug Delivery Rev.* **2012**, *64*, 206–212.
6. Owens, D. E.; Peppas, N. A. Opsonization, Biodistribution, and Pharmacokinetics of Polymeric Nanoparticles. *Int. J. Pharm.* **2006**, *307*, 93–102.
7. Kaminskas, L. M.; McLeod, V. M.; Kelly, B. D.; Sberna, G.; Boyd, B. J.; Williamson, M.; Owen, D. J.; Porter, C. J. A Comparison of Changes to Doxorubicin Pharmacokinetics, Antitumor Activity, and Toxicity Mediated by PEGylated Dendrimer and PEGylated Liposome Drug Delivery Systems. *Nanomedicine* **2012**, *8*, 103–111.
8. Mitchell, N.; Kalber, T. L.; Cooper, M. S.; Sunassee, K.; Chalker, S. L.; Shaw, K. P.; Ordidge, K. L.; Badar, A.; Janes, S. M.; Blower, P. J.; *et al.* Incorporation of Paramagnetic, Fluorescent and PET/SPECT Contrast Agents into Liposomes for Multimodal Imaging. *Biomaterials* **2013**, *34*, 1179–1192.
9. Torchilin, V. P. Recent Advances with Liposomes as Pharmaceutical Carriers. *Nat. Rev. Drug Discovery* **2005**, *4*, 145–160.
10. Minchinton, A. I.; Tannock, I. F. Drug Penetration in Solid Tumours. *Nat. Rev. Cancer* **2006**, *6*, 583–592.
11. Heldin, C. H.; Rubin, K.; Pietras, K.; Ostman, A. High Interstitial Fluid Pressure—An Obstacle in Cancer Therapy. *Nat. Rev. Cancer* **2004**, *4*, 806–813.
12. Brown, J. M.; William, W. R. Exploiting Tumour Hypoxia in Cancer Treatment. *Nat. Rev. Cancer* **2004**, *4*, 437–447.
13. Harrison, L.; Blackwell, K. Hypoxia and Anemia: Factors in Decreased Sensitivity to Radiation Therapy and Chemotherapy? *Oncologist* **2004**, *9*, 31–40.
14. Martel, S. Magnetic Therapeutic Delivery Using Navigable Agents. *Ther. Delivery* **2014**, *5*, 189–204.
15. Forbes, N. S. Engineering the Perfect (Bacterial) Cancer Therapy. *Nat. Rev. Cancer* **2010**, *10*, 784–793.
16. Ganai, S.; Arenas, R. B.; Sauer, J. P.; Bentley, B.; Forbes, N. S. In Tumors Salmonella Migrate Away from Vasculature toward the Transition Zone and Induce Apoptosis. *Cancer Gene Ther.* **2011**, *18*, 457–466.
17. Koumoutsakos, P.; Pivkin, I.; Milde, F. The Fluid Mechanics of Cancer and Its Therapy. *Annu. Rev. Fluid Mech.* **2013**, *45*, 325–355.
18. Felfoul, O.; Mathieu, J. B.; Martel, S. In *A Comparative Study between MC-1 Cells and Magnetic Microparticles Used for Enhanced Target Delivery of Therapeutic Agents in the Microvasculature*, 2nd ed.; Biennial P IEEE Ras-Embs Int.: Scottsdale, AZ, 2008; pp 694−699.
19. Martel, S.; Mohammadi, M.; Felfoul, O.; Lu, Z.; Pouponneau, P. Flagellated Magnetotactic Bacteria as Controlled MRI-Trackable Propulsion and Steering Systems for Medical Nanorobots Operating in the Human Microvasculature. *Int. J. Rob. Res.* **2009**, *28*, 571–582.
20. Martel, S. Navigation Control of Micro-Agents in the Vascular Network: Challenges and Strategies for Endovascular Magnetic Navigation Control of Microscale Drug Delivery Carriers. *IEEE Control Syst.* **2013**, *33*, 119–134.
21. McDonald, D. M.; Baluk, P. Significance of Blood Vessel Leakiness in Cancer. *Cancer Res.* **2002**, *62*, 5381–5385.
22. Frankel, R. B.; Bazylinski, D. A.; Johnson, M. S.; Taylor, B. L. Magneto-Aerotaxis in Marine Coccoid Bacteria. *Biophys. J.* **1997**, *73*, 994–1000.
23. Faivre, D.; Schuler, D. Magnetotactic Bacteria and Magnetosomes. *Chem. Rev.* **2008**, *108*, 4875–4898.
24. Arakaki, A.; Nakazawa, H.; Nemoto, M.; Mori, T.; Matsunaga, T. Formation of Magnetite by Bacteria and Its Application. *J. R. Soc., Interface* **2008**, *5*, 977–999.
25. De Lanauze, D.; Felfoul, O.; Turcot, J. P.; Mohammadi, M.; Martel, S. Three-Dimensional Remote Aggregation and Steering of Magnetotactic Bacteria Microrobots for Drug Delivery Applications. *Int. J. Rob. Res.* **2013**, 1–16.
26. Schulz, G. E. The Structure of Bacterial Outer Membrane Proteins. *Biochim. Biophys. Acta* **2002**, *1565*, 308–317.
27. Sun, J.; Li, Y.; Liang, X. J.; Wang, P. C. Bacterial Magnetosome: A Novel Biogenetic Magnetic Targeted Drug Carrier with Potential Multifunctions. *J. Nanomater.* **2011**, *2011*, 469031–469043.
28. Kalia, J.; Raines, R. T. Advances in Bioconjugation. *Curr. Org. Chem.* **2010**, *14*, 138–147.
29. Hermanson, G. T. *Bioconjugate Techniques*, 2nd ed.; Elsevier Academic Press: Amsterdam, Boston, 2008.
30. Stephan, M. T.; Moon, J. J.; Um, S. H.; Bershteyn, A.; Irvine, D. J. Therapeutic Cell Engineering with Surface-Conjugated Synthetic Nanoparticles. *Nat. Med.* **2010**, *16*, 1035–1041.
31. Berry, C. C. Progress in Functionalization of Magnetic Nanoparticles for Applications in Biomedicine. *J. Phys. D: Appl. Phys.* **2009**, *42*, 1–9.
32. Sun, C.; Lee, J. S. H.; Zhang, M. Q. Magnetic Nanoparticles in MR Imaging and Drug Delivery. *Adv. Drug Delivery Rev.* **2008**, *60*, 1252–1265.
33. Lang, C.; Schuler, D.; Faivre, D. Synthesis of Magnetite Nanoparticles for Bio- and Nanotechnology: Genetic Engineering and Biomimetics of Bacterial Magnetosomes. *Macromol. Biosci.* **2007**, *7*, 144–151.
34. Veiseh, O.; Gunn, J. W.; Zhang, M. Q. Design and Fabrication of Magnetic Nanoparticles for Targeted Drug Delivery and Imaging. *Adv. Drug Delivery Rev.* **2010**, *62*, 284–304.
35. Martel, S. Combining Pulsed and DC Gradients in a Clinical MRI-Based Microrobotic Platform to Guide Therapeutic

Magnetic Agents in the Vascular Network. *Int. J. Adv. Rob. Syst.* **2013**, *10*, 1–7.
36. Klabunde, R. E. *Cardiovascular Physiology Concepts*, 2nd ed.; Lippincott Williams & Wilkins: Philadelphia, PA, 2011.
37. Jiang, W.; Saxena, A.; Song, B.; Ward, B. B.; Beveridge, T. J.; Myneni, S. C. B. Elucidation of Functional Groups on Gram-Positive and Gram-Negative Bacterial Surfaces Using Infrared Spectroscopy. *Langmuir* **2004**, *20*, 11433–11442.
38. Silhavy, T. J.; Kahne, D.; Walker, S. The Bacterial Cell Envelope. *Cold Spring Harbor Perspect. Biol.* **2010**, *2*, 1–26.
39. Gao, X.; Cui, Y.; Levenson, R. M.; Chung, L. W.; Nie, S. *In Vivo* Cancer Targeting and Imaging with Semiconductor Quantum Dots. *Nat. Biotechnol.* **2004**, *22*, 969–976.
40. Farokhzad, O. C.; Cheng, J.; Teply, B. A.; Sherifi, I.; Jon, S.; Kantoff, P. W.; Richie, J. P.; Langer, R. Targeted Nanoparticle-Aptamer Bioconjugates for Cancer Chemotherapy *in Vivo*. *Proc. Natl. Acad. Sci. U. S. A.* **2006**, *103*, 6315–6320.
41. Meyer, R. L.; Zhou, X. F.; Tang, L. N.; Arpanaei, A.; Kingshott, P.; Besenbacher, F. Immobilisation of Living Bacteria for AFM Imaging under Physiological Conditions. *Ultramicroscopy* **2010**, *110*, 1349–1357.
42. Luo, Y. R. *Comprehensive Handbook of Chemical Bond Energies*; CRC Press, Taylor and Francis Group: Boca Raton, FL, 2007.
43. Garrett, H. R.; Grisham, C. M. *Biochemistry*, 5th ed.; Brooks/Cole, Cengage Learning: Belmont, CA, 2012.
44. Huang, Y. F.; Wang, Y. F.; Yan, X. P. Amine-Functionalized Magnetic Nanoparticles for Rapid Capture and Removal of Bacterial Pathogens. *Environ. Sci. Technol.* **2010**, *44*, 7908–7913.
45. Marttila, A. T.; Laitinen, O. H.; Airenne, K. J.; Kulik, T.; Bayer, E. A.; Wilchek, M.; Kulomaa, M. S. Recombinant Neutralite Avidin: A Non-Glycosylated, Acidic Mutant of Chicken Avidin That Exhibits High Affinity for Biotin and Low Non-Specific Binding Properties. *FEBS Lett.* **2000**, *467*, 31–36.
46. Thorek, D. L. J.; Elias, D. R.; Tsourkas, A. Comparative Analysis of Nanoparticle-Antibody Conjugations: Carbodiimide *versus* Click Chemistry. *Mol. Imaging* **2009**, *8*, 221–229.
47. Danila, D.; Partha, R.; Elrod, D. B.; Lackey, M.; Casscells, S. W.; Conyers, J. L. Antibody-Labeled Liposomes for CT Imaging of Atherosclerotic Plaques: *In Vitro* Investigation of an Anti-ICAM Antibody-Labeled Liposome Containing Iohexol for Molecular Imaging of Atherosclerotic Plaques *via* Computed Tomography. *Tex. Heart Inst. J.* **2009**, *36*, 393–403.
48. Martin, R. B. Free Energies and Equilibria of Peptide Bond Hydrolysis and Formation. *Biopolymers* **1998**, *45*, 351–353.
49. Osaka, T.; Nakanishi, T.; Shanmugam, S.; Takahama, S.; Zhang, H. Effect of Surface Charge of Magnetite Nanoparticles on Their Internalization into Breast Cancer and Umbilical Vein Endothelial Cells. *Colloid Surf. B* **2009**, *71*, 325–330.
50. Marquez, M.; Nilsson, S.; Lennartsson, L.; Liu, Z. X.; Tammela, T.; Raitanen, M.; Holmberg, A. R. Charge-Dependent Targeting: Results in Six Tumor Cell Lines. *Anticancer Res.* **2004**, *24*, 1347–1351.
51. Miller, C. R.; Bondurant, B.; McLean, S. D.; McGovern, K. A.; O'Brien, D. F. Liposome-Cell Interactions *in Vitro*: Effect of Liposome Surface Charge on the Binding and Endocytosis of Conventional and Sterically Stabilized Liposomes. *Biochemistry* **1998**, *37*, 12875–12883.
52. Garcia-Perez, B. E.; De la Cruz-Lopez, J. J.; Castaneda-Sanchez, J. I.; Munoz-Duarte, A. R.; Hernandez-Perez, A. D.; Villegas-Castrejon, H.; Garcia-Latorre, E.; Caamal-Ley, A.; Luna-Herrera, J. Macropinocytosis Is Responsible for the Uptake of Pathogenic and Non-Pathogenic Mycobacteria by B Lymphocytes (Raji Cells). *BMC Microbiol.* **2012**, *12*, 1–14.
53. Garcia-Perez, B. E.; Hernandez-Gonzalez, J. C.; Garcia-Nieto, S.; Luna-Herrera, J. Internalization of a Non-Pathogenic Mycobacteria by Macropinocytosis in Human Alveolar Epithelial A549 Cells. *Microb. Pathog.* **2008**, *45*, 1–6.
54. Andar, A. U.; Hood, R. R.; Vreeland, W. N.; Devoe, D. L.; Swaan, P. W. Microfluidic Preparation of Liposomes to Determine Particle Size Influence on Cellular Uptake Mechanisms. *Pharm. Res.* **2013**, *31*, 401–413.
55. Martina, M. S.; Nicolas, V.; Wilhelm, C.; Meenager, C.; Barratt, G.; Lesieur, S. The *in Vitro* Kinetics of the Interactions between PEG-ylated Magnetic-Fluid-Loaded Liposomes and Macrophages. *Biomaterials* **2007**, *28*, 4143–4153.
56. Hoskin, D. W.; Ramamoorthy, A. Studies on Anticancer Activities of Antimicrobial Peptides. *Biochim. Biophys. Acta* **2008**, *1778*, 357–375.
57. Immordino, M. L.; Dosio, F.; Cattel, L. Stealth Liposomes: Review of the Basic Science, Rationale, and Clinical Applications, Existing and Potential. *Int. J. Nanomed.* **2006**, *1*, 297–315.
58. Bazylinski, D. A.; Williams, T. J.; Lefevre, C. T.; Berg, R. J.; Zhang, C. L. L.; Bowser, S. S.; Dean, A. J.; Beveridge, T. J. Magnetococcus Marinus gen. nov., sp nov., a Marine, Magnetotactic Bacterium That Represents a Novel Lineage (Magnetococcaceae fam. nov., Magnetococcales ord. nov.) at the Base of the Alphaproteobacteria. *Int. J. Syst. Evol. Microbiol.* **2013**, *63*, 801–808.
59. Ngamwongsatit, P.; Banada, P. P.; Panbangred, W.; Bhunia, A. K. WST-1-Based Cell Cytotoxicity Assay as a Substitute for MTT-Based Assay for Rapid Detection of Toxigenic Bacillus Species Using Cho Cell Line. *J. Microbiol. Methods* **2008**, *73*, 211–215.